Minimum S-Excess Graph for Segmenting and Tracking Multiple Borders with HMM*

Ehab Essa, Xianghua Xie**, and Jonathan-Lee Jones

Department of Computer Science, Swansea University, UK
x.xie@swan.ac.uk

Abstract. We present a novel HMM based approach to simultaneous segmentation of vessel walls in Lymphatic confocal images. The vessel borders are parameterized using RBFs to minimize the number of tracking points. The proposed method tracks the hidden states that indicate border locations for both the inner and outer walls. The observation for both borders is obtained using edge-based features from steerable filters. Two separate Gaussian probability distributions for the vessel borders and background are used to infer the emission probability, and the transmission probability is learned using a Baum-Welch algorithm. We transform the segmentation problem into a minimization of an s-excess graph cost, with each node in the graph corresponding to a hidden state and the weight for each node being defined by its emission probability. We define the inter-relations between neighboring nodes based on the transmission probability. We present both qualitative and quantitative analysis in comparison to the popular Viterbi algorithm.

1 Introduction

Tracking object contour is usually carried out for complex and nonrigid shapes where a contour provides more accurate representation than a bounding box. In this paper, we propose a hidden Markov model (HMM) based approach to track lymphatic anatomical borders over the cross-sectional images in order to achieve coherent segmentations in 3D. HMM is a stochastic model in which the Markov property is assumed to be satisfied in a finite set of states and these states are hidden. Many applications have demonstrated the advantages of HMM in dealing with time-varying series, such as [3,4,14]. In [11], the authors used HMM to detect abnormal local wall motion in stress echocardiography. In [5], HMM is used in conjunction with a particle filter to track hand motion. The particle filter is used to estimate the hand region that is most likely to appear. HMM estimates the hand shape using the Viterbi algorithm where the hidden state is a set of quantized pre-learned exemplars. However, the number of exemplars can grow exponentially depending on the complexity of the object. In [2], the authors

* The project is funded by NISCHR MIAV-BRU. E. Essa was funded by Swansea University as a PhD student and NISCHR as a postdoc, and he is also affiliated with Mansoura University, Egypt.

** Corresponding author.

N. Navab et al. (Eds.): MICCAI 2015, Part II, LNCS 9350, pp. 28–35, 2015.
DOI: 10.1007/978-3-319-24571-3_4

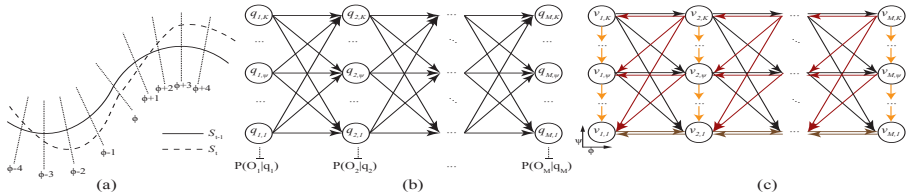

Fig. 1. (a) an illustration of segmenting border S_t based on S_{t-1}. The border is divided into M points with RBF interpolation and at each point a normal line is drawn with length K. (b) conventional HMM construction. (c) proposed HMM construction.

used the Kalman filter with pseudo 2-dimensional HMM to perform tracking. The Viterbi algorithm is used to find the best sequence of states to perform object and background classification. However, this system becomes increasingly more complex and time-consuming with the increase of object size. In [3,4], the authors incorporated region and edge features in HMM. The contour is sampled as a set of discrete points, and the features are extracted along the normal direction at each contour point. An ellipse is fitted to the contour and the unscented Kalman filter is used for tracking. Sargin *et al.* [14] extended the work to deal with variable length open contours and investigated using arc emission instead of traditional state emission in defining the observational probabilities for the HMM. Notably, Viterbi algorithm is commonly used to find the best sequence of hidden states. However, the search process can be hampered by occlusions in the image where the emission probability is not reliable and transition probability does not guarantee smooth transition of the border. Moreover, the Viterbi algorithm cannot handle the case when starting and ending points are the same. Nor does it work well to simultaneously search multiple borders.

In this paper, we propose a multi-border segmentation and tracking method based on HMM, and we demonstrate the technique through simultaneously delineating the inner and outer borders in lymphatic vessel images that are corrupted by noise, intensity inhomogeneity and occlusions. A new optimization method is proposed to find the optimal sequence of the hidden states based on the minimization of an s-excess graph. Instead of using the traditional Viterbi algorithm, we transform the problem into finding the minimum-cost closet set graph that corresponds to the desired border and can be efficiently solved in polynomial time. The emission probability is defined based on two probability distributions of the vessel border and background respectively that are derived directly from edge-based features. The training of the transition probability is achieved by using the Baum-Welch algorithm.

2 Proposed Method

2.1 Border Parameterization

The border of interest can be either an open curve/surface or a closed contour/surface. For the purpose of efficient graph optimization, we unravel the

images so that the border of interest appears to be an open contour in 2D or an open surface in 3D. The first columns and the last columns of the image data are connected so that the continuity of the original data is unaffected. In effect, the images are transformed from Cartesian coordinates to polar coordinates. This is particularly suitable for vessel segmentation. We thus treat the segmentation of the two vessel walls in 3D as tracking two non-overlapping and non-crossing contours in the longitudinal direction. Compared to the optimal surface method [9], which also adopts image unravelling, our approach has very limited computational overhead when dealing with 3D data in that only adjacent cross sections are needed to construct the graph for segmentation. We further simplify the border of interest in 2D cross sections through radial basis function (RBF) based parameterization, since it is unnecessary to track each every point along the boarder. As illustrated in Fig. 1(a), the border of interest is approximated by RBFs where the hidden states of the HMM are considered as the potential RBF centers. The border is evenly sampled into M points and at each point a line segment is drawn perpendicular to the tangent line of the border and each line segment has K points. The RBF centers are indexed by $\phi \in \{1, \ldots, M\}$ and points on perpendicular line segments are indexed by $\psi \in \{1, \ldots, K\}$. The initial RBF centers for the current cross section or frame are defined using the result from the previous frame, see Fig. 1(a).

2.2 HMM Formulation

The segmentation of both vessel walls in 3D is then transformed into tracking of two sets of RBF centers in longitudinal direction. For the proposed HMM, we denote all possible sequences of hidden states as $Q = \{q\}$, where $q = \{q_1, \ldots, q_\phi, \ldots, q_M\}$ is one possible state sequence and q_ϕ is the state on the normal at ϕ. These sequences correspond to possible RBF center locations. The HMM observations $O = \{O_1, \ldots, O_\phi, \ldots, O_M\}$ are extracted from the normal lines. HMM is specified by three probability measures $\lambda = (A, B, \pi)$, where A, B and π are the probabilities for the transition, emission and initial states. The transition between states q at two normals ϕ and $\phi + 1$ are governed by a set of probabilities, i.e. transition probabilities $P(q_\phi | q_{\phi+1})$, and any state can only be observed by an output event according to associated probability distribution, i.e. emission probabilities $P(O_\phi | q_\phi)$. The output event is the image features extracted from each state at the normal line.

Image observations are modeled by two probability density functions: one for the vessel wall and the other for the background. Let $O_\phi = \{o_{\phi,1}, \ldots, o_{\phi,\psi}, \ldots, o_{\phi,K}\}$ be a set of features along the normal ϕ and $o_{\phi,\psi}$ a feature extracted from point ψ on the line. $P(o_{\phi,\psi}|F)$ and $P(o_{\phi,\psi}|B)$ represent the probabilities of that feature belonging to the border of interest and the background respectively. The state-emission probability is defined as: $P(O_\phi|q_\phi) \propto P(o_{\phi,\psi}|F) \prod_{\psi \neq q_\phi} P(o_{\phi,\psi}|B)$. The likelihood of the observed variables O_ϕ from a state q_ϕ is computed by measuring the likelihood of each feature $o_{\phi,\psi}$ at index ψ on the line ϕ belonging to the contour and all the rest of features on that

line belonging to the background. From a set of training data with a manually labeled borders of interest, we use first order derivatives of Gaussian filters [6] in six different orientations to highlight the edge features along the border, and extract features that correspond to the border and the background, in order to learn the mean and variance of two Gaussian distributions $P(F)$ and $P(B)$.

For the transition probability, we use the Baum-Welch (Forward-Backward) algorithm [13] to learn both the transition and initial probabilities. The process is iterative and each iteration increases the likelihood of the data $P(O|\hat{\lambda}) \geq P(O|\lambda)$ until convergence. Note the emission probability is already computed as described before and there is no need for it to be re-estimated. The initial probability is only needed in case of Viterbi algorithm is used.

2.3 Minimum S-Excess Graph Optimization

Minimization of closure graph and s-excess problems have been applied in image segmentation, e.g. [9,15]. In [9], the authors formulated the problem as a minimization of a closed graph to find the optimal surfaces on d-dimensional multi-column graphs ($d \geq 3$). However, only weighted graph nodes is used in the segmentation by assuming the surface is changing within a global constant constraint which is difficult to define and may lead to abrupt changes of the surface due to its sensitivity to nodal weights. Recently, its graph construction has been extended to handle volumetric data without image unravelling. For example, in [12], Petersen *et al.* proposed to use graph columns defined from non-intersecting, non-parallel flow lines obtained from an initial segmentation. In [15], prior information is incorporated by encoding the prior shapes as a set of convex functions defined between every pair of adjacent columns. Our work is similar to Song *et al.* [15] in that aspect. However, we formulate the problem as tracking borders in consecutive frames, i.e. defining the pair-wise cost based on the transition probability learned from the training data and treating it as a stochastic process, whilst the optimal surface method searches the border as a surface in volumetric image, which is much more computationally expensive. Moreover, the proposed method can tackle more complex shapes, such as open, closed, and variable length contours.

The minimum s-excess problem [8] is a relaxation of minimum closure set problem. A closed set is a subset of graph where all successors of any nodes in the set are also taken in the set. The successors of nodes may not be contained in the set but with their cost equal to the edge costs heading to such successors. Given a directed graph $G(V, E)$, each node $v \in V$ is assigned to a certain weight $w(v)$ and each edge $e \in E$ have a positive cost. The task is to obtain a subset of graph nodes $S \subset V$ where the total nodal cost and the cost of separating the set from the rest of the graph $S' = V - S$ are minimized: $\mathcal{E} = \sum_{v \in S} w(v) + \sum_{\substack{(u,v) \in E \\ u \in S, v \in S'}} c(u, v)$.

For each border of interest $\mathcal{S}$, a graph G_s is constructed in $M \times K$. Each node in the graph corresponds to one hidden state and each normal line is referred to as a column chain. We have three type of graph arcs: intra-chain, inter-chain and inter-border arcs as shown in Fig. 1(c). For intra-chain, along each chain

$C(\phi,\psi)$, every node $v(\phi,\psi)$ ($\phi \in \{1,\ldots,M\}$, $\psi \in \{1,\ldots,K\}$, and here $\psi > 1$) has a directed arc to the node $v(\phi,\psi-1)$ with $+\infty$ weight assigned to the edge to ensure that the desired border intersects with each chain once and once only. In the case of inter-chain, for every pair of adjacent chains $C(\phi_1,\psi_1)$ and $C(\phi_2,\psi_2)$, a set of directed arcs are established to link node $v(\phi_1,\psi_1)$ to nodes $v(\phi_2,\psi_2')$ in $C(\phi_2,\psi_2)$, where $1 \leq \psi_2' \leq \psi_1$. Similarly, directed arcs are used to link node $v(\phi_2,\psi_2)$ to node $v(\phi_1,\psi_1')$ in the $C(\phi_1,\psi_1)$ where $1 \leq \psi_1' \leq \psi_2$. Since each hidden state is represented by a node in the graph, the cost of arcs between a pair of adjacent chains is defined by the HMM transition matrix $A(q_{\phi_1,\psi_1}, q_{\phi_2,\psi_2})$. The last row of each graph is connected to each other to form the base of the closed graph. Since the images are unravelled into the polar coordinates, the first and last chains are also connected in the same manner as the inter-chain arcs to ensure connectivity. Inter-border arcs are defined to impose the non-overlapping constraint between two vessel borders, i.e. $\underline{\Delta} \leq \mathcal{S}_1 - \mathcal{S}_2 \leq \bar{\Delta}$. Let $C_1(\phi,\psi)$ and $C_2(\phi,\psi)$ denote two corresponding chains from G_1 and G_2, $\hat{\psi}$ be the spatial coordinate equivalent to ψ in the graph domain, and $X \times Y$ denote the spatial domain size. For any node $v_1(\phi,\hat{\psi})$ in $C_1(\phi,\psi)$, a direct arc is established between $v_1(\phi,\hat{\psi})$ and $v_2(\phi,\hat{\psi}-\bar{\Delta})$ where $\hat{\psi} \geq \bar{\Delta}$ and $v_2 \in C_2(\phi,\psi)$. Also, nodes $v_2(\phi,\hat{\psi})$ in $C_2(\phi,\psi)$ are connected to $v_1(\phi,\hat{\psi}+\underline{\Delta})$ where $\hat{\psi} < Y - \underline{\Delta}$ and $v_1 \in C_1(\phi,\psi)$. The cost of these arcs is assigned as $+\infty$ such that the minimum and maximin distances are imposed as hard constraints.

Fig. 1(b,c) shows the comparison between the conventional HMM and the proposed HMM construction. The intra-chain arcs and the arcs in the last row are necessary in order to compute the closed set graph. The transition between states is defined as a set of inter-chain arcs from left-to-right and right-to-left to ensure that the cost of cut is proportional to the distance of border location between two neighboring chains.

The emission probability for every node is converted to graph cost according to $W(\phi,\psi) = -log(P(o_{\phi,\psi}|q_{\phi,\psi}))$ and it is inversely proportional to the likelihood that the border of interest passes through the node (ϕ,ψ). The weight for each node $w(\phi,\psi)$ on the directed graph is defined as $w(\phi,\psi) = W(\phi,\psi) - W(\phi,\psi-1)$, except for the bottom chain, i.e. $w(\phi,1) = W(\phi,1)$. Hochbaum [7] showed that the minimum s-excess problem is equivalent to solving the minimum $s-t$ cut [1] defined on a proper graph. Hence, the s-t cut algorithm is used to find the minimum closed set in polynomial time. The cost of the cut is the total edge cost in separating the graph into source and sink sets.

Table 1. Inner border quantitative results (mean value and standard deviation).

	AMD	HD	AO	Sens.	Spec.
Optimal Surface [9]	7.1 ± 3.5	50.6 ± 22.1	90.1 ± 5.6	91.2 ± 5.6	99.3 ± 0.6
Using Viterbi Alg.	35.4 ± 18.5	82.2 ± 17.7	53.1 ± 20.9	53.2 ± 21.0	$\mathbf{99.9 \pm 0.1}$
Single border s-excess	4.9 ± 3.2	15.6 ± 10.0	93.0 ± 4.9	93.6 ± 4.9	99.6 ± 0.6
Double border s-excess	$\mathbf{3.1 \pm 1.9}$	$\mathbf{9.8 \pm 4.3}$	$\mathbf{95.5 \pm 3.2}$	$\mathbf{96.9 \pm 3.1}$	99.2 ± 0.8

Table 2. Outer border quantitative results (mean value and standard deviation).

	AMD	HD	AO	Sens.	Spec.
Optimal Surface [9]	7.0 ± 5.9	54.9 ± 26.1	91.7 ± 7.3	92.7 ± 7.5	99.2 ± 0.5
Using Viterbi Alg.	3.2 ± 1.2	13.6 ± 5.6	96.4 ± 1.3	97.6 ± 1.3	98.9 ± 1.3
Single border s-excess	2.4 ± 0.8	8.1 ± 3.7	97.2 ± 1.2	97.8 ± 1.3	$\mathbf{99.5 \pm 0.5}$
Double border s-excess	$\mathbf{2.0 \pm 0.8}$	$\mathbf{7.4 \pm 3.1}$	$\mathbf{97.6 \pm 1.0}$	$\mathbf{98.7 \pm 1.1}$	99.1 ± 0.6

3 Application and Results

The proposed method is applied to segmenting lymphatic vessel images that are obtained using confocal microscopy. Confocal microscopy is a method that allows for the visualization and imaging of 3D volume objects that are thicker than the focal plane of a conventional microscope. For the purpose of our evaluation, a total of 48 segments were obtained from in vitro confocal microscopy images and 16 of those were randomly selected for training the HMM. Anisotropic vessel diffusion [10] was applied to enhance image features and to improve vessel connectivity, as well as to reduce the amount of image noise that is typical in this type of images. Each 3D segment is measured at $512 \times 512 \times 512$ voxels. The evaluation was carried out on every frame where manual labeling was performed. Five different evaluation metrics were used, i.e. absolute mean difference (AMD), Hausdorff distance (HD) in pixel, sensitivity (Sens. %), specificity (Spec. %), and Area Overlap (AO %). The inner region is considered as positive for Sens. and Spec. measurements. The normal line segments were measured at a length of 101 pixels, and 42 RBF centers in polar coordinates were used, i.e. one RBF centre every 30 pixels. The minimum and maximum distance between two borders, $\underline{\Delta}$ and $\bar{\Delta}$, are fixed to 5 and 25 respectively.

Tables 1 and 2 present the quantitative results of segmenting both the inner and outer vessel walls, respectively. Some typical segmentation results are shown in Fig. 2. The proposed s-excess optimization clearly outperformed the Viterbi algorithm in tracking both borders. The Viterbi based method was easily distracted by lymphatic valves attached to the inner wall and produced high distance error and low sensitivity. It also requires a much larger amount of data to train the transition and prior probabilities. The proposed method was also compared against the optimal surface segmentation [9]. The results of the optimal surface method were found sensitive to the distance parameters between columns. The proposed method has full connection of arcs between chains and produced better and more consistent results. The result of simultaneous segmentation of both borders was found better than segmenting the borders separately. Particularly for inner border segmentation (shown in Table 1), the inter-border constraint significantly improved its performance against distraction from lymphatic valves. The proposed s-excess optimization also achieved much smoother border transition, particularly when there was an occlusion or missing feature (see Fig. 2). Fig. 3 shows 3D visualization of some segmentation results.

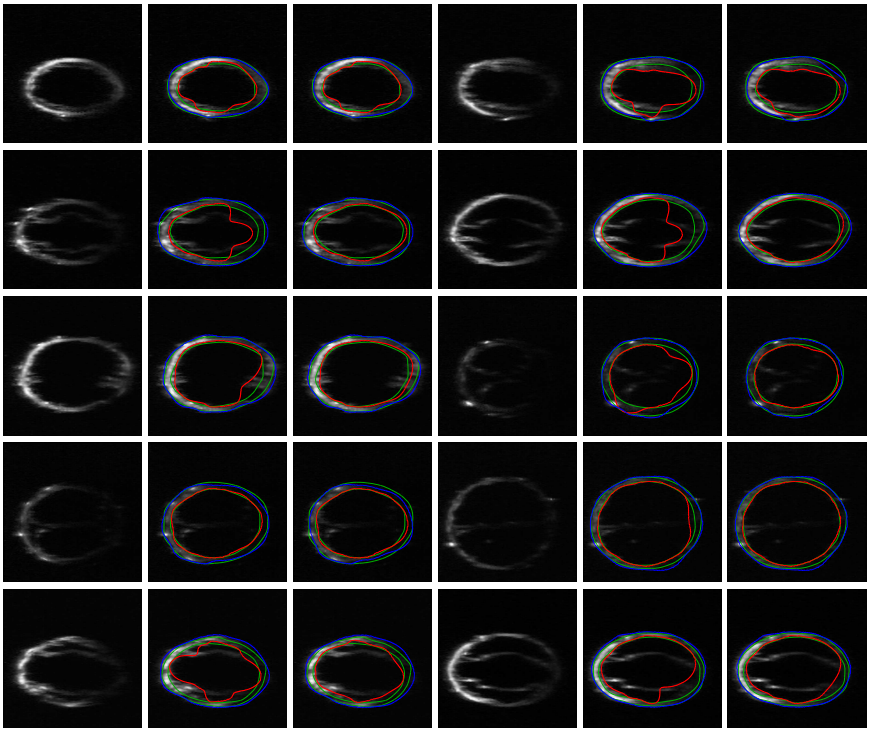

Fig. 2. Comparison between ground-truth (green) and segmentation results (red: inner, blue: outer). (a,d) original image (b,e) proposed single border method. (c,f) proposed double border method.

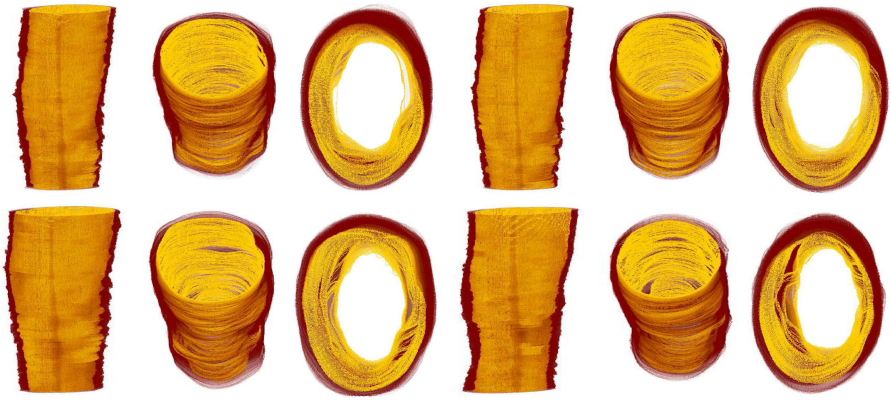

Fig. 3. Visualization of the results in 3D by the proposed method (inner wall: yellow, outer wall: red).

4 Conclusions

We presented an HMM based method for simultaneously segmenting the inner and outer lymphatic vessel borders in confocal images. The method searches for the border along a set of normal lines based on the segmentation of the previous frame. Boundary based features were extracted to infer the emission probability. We show that the optimal sequence of the hidden states corresponds to RBFs of the border can be effectively obtained by solving a minimum s-excess problem. Qualitative and quantitative results on lymphatic images showed the superior performance of the proposed method.

Acknowledgement. The authors like thank D. Zawieja for the data.

References

1. Boykov, Y., Kolmogorov, V.: An experimental comparison of min-cut/max-flow algorithms for energy minimization in vision. IEEE PAMI 26(9), 1124–1137 (2004)
2. Breit, H., Rigoll, G.: Improved person tracking using a combined pseudo-2D-HMM and kalman filter approach with automatic background state adaptation. In: ICIP (2001)
3. Chen, Y., Rui, Y., Huang, T.S.: JPDAF based HMM for real-time contour tracking. In: CVPR (2001)
4. Chen, Y., Rui, Y., Huang, T.S.: Multicue HMM-UKF for real-time contour tracking. IEEE PAMI 28(9), 1525–1529 (2006)
5. Fei, H., Reid, I.D.: Joint bayes filter: A hybrid tracker for non-rigid hand motion recognition. In: Pajdla, T., Matas, J(G.) (eds.) ECCV 2004. LNCS, vol. 3023, pp. 497–508. Springer, Heidelberg (2004)
6. Freeman, W.T., Adelson, E.H.: The design and use of steerable filters. IEEE PAMI 13(9), 891–906 (1991)
7. Hochbaum, D.: An efficient algorithm for image segmentation, markov random fields and related problems. J. ACM 48(4), 686–701 (2001)
8. Hochbaum, D.: Anniversary article: Selection, provisioning, shared fixed costs, maximum closure, and implications on algorithmic methods today. Manage. Sci. 50(6), 709–723 (2004)
9. Li, K., Wu, K., Chen, D.Z., Sonka, M.: Optimal surface segmentation in volumetric images-a graph-theoretic approach. IEEE PAMI 28(1), 119–134 (2006)
10. Manniesing, R., Viergever, M., Niessen, W.: Vessel enhancing diffusion: A scale space representation of vessel structures. MIA 10(6), 815 (2006)
11. Mansor, S., Noble, J.A.: Local wall motion classification of stress echocardiography using a hidden markov model approach. In: ISBI (2008)
12. Petersen, J., et al.: Optimal surface segmentation using flow lines to quantify airway abnormalities in chronic obstructive pulmonary disease. MIA 18, 531–541 (2014)
13. Rabiner, L.: A tutorial on hidden markov models and selected applications in speech recognition. Proceedings of the IEEE 77(2), 257–286 (1989)
14. Sargin, M.E., Altinok, A., Manjunath, B.S., Rose, K.: Variable length open contour tracking using a deformable trellis. IEEE TIP 20(4), 1023–1035 (2011)
15. Song, Q., et al.: Optimal multiple surface segmentation with shape and context priors. IEEE TMI 32(2), 376–386 (2013)